

Temperature variation of the size effect in dilute AlMg and AlCa alloys: Measurement and theory

H. M. Gilder*

Section d'Etudes des Solides Irradiés, Centre d'Etudes Nucléaires, 92260 Fontenay-aux-Roses, France

M. Asty†

Section d'Etudes des Solides Irradiés, Centre d'Etudes Nucléaires, 92260 Fontenay-aux-Roses, France

Ph. Audit

Laboratoire des Propriétés Mécaniques et Thermodynamiques des Matériaux, Université Paris-Nord, Avenue J. B. Clément, 93430 Villetaneuse, France

(Received 11 March 1980)

Optical-interferometric-differential-length and x-ray lattice-parameter measurements performed at low temperatures in dilute AlMg and AlCa alloys indicate that the temperature variation of the size effect corresponds to a relatively large difference between the intrinsic coefficient of thermal expansion β_i of the solute atom structure and that, β , of the solvent. This result is another example of the surprising expansive properties of point defects previously described by Gilder and co-workers (high-temperature vacancy diffusion) and more recently by Ganne (low-temperature dilatometry on irradiated specimens). Specifically, in the temperature range $0.2 < T/\Theta_D < 0.4$, we find that $\beta_i(\text{Mg})/\beta \approx 3$ and $\beta_i(\text{Ca})/\beta \approx -4$. This, as well as the fact that the sign of the change in the coefficient of thermal expansion $\Delta\beta$ of the host metal caused by the introduction of the solute atom is positive for Mg and negative for Ca, indicates that solute-solvent valence effects play a minor role in determining the coefficient of thermal expansion of the dilute alloy. It is also found, to within the experimental precision, that $\Delta\beta(\text{Mg})$ and $\Delta\beta(\text{Ca})$ are temperature independent, suggesting a type of Matthiessen's rule for thermal expansion. A model calculation of the size effect and its temperature variation in the infinitely dilute alloy is presented. The volume-dependent forces are treated by means of a term describing the elastic energy associated with the solute-solvent volume misfit, whereas the temperature-dependent potential of Dagens *et al.* is used to calculate the pairwise interaction between the solvent ions and the solute ion. Good agreement with the experimental data is obtained for the size effect in both AlMg and AlCa. The calculated values of $\Delta\beta(\text{Mg})/C_i$, C_i being the solute concentration, and $\beta_i(\text{Mg})$ fall between the measured values in the two AlMg alloys studied. The calculation of $\Delta\beta(\text{Ca})/C_i$ and $\beta_i(\text{Ca})$ is not possible due to a lack of elastic-constants data for pure, metallic calcium. Inasmuch as, in the case of Mg, solute-solute interactions are apparent in the measured values of the size effect, $\Delta\beta/C_i$ and β_i , even at $C_i(\text{Mg}) \sim 0.2$ at.%, extreme care must be exercised when comparing experimental data for dilute alloys with calculations of infinitely dilute alloy properties.

I. INTRODUCTION

The change in volume Ω_i accompanying the insertion of a substitutional impurity or vacancy in a metallic host crystal of atomic volume Ω defines the physically measurable quantity commonly referred to as the size effect or fractional defect formation volume Ω_i/Ω . Although calculations of the vacancy size effect are numerous,¹ calculations of its temperature variation, and hence of the change in thermal expansion $\Delta\beta_i$ of the host metal on alloying with vacancies, are indeed less abundant.²⁻⁴ When $\Delta\beta_i$ is much larger than expected,^{5,6} or equivalently, when the intrinsic coefficient of thermal expansion β_i of the vacancy is much greater than the coefficient of thermal expansion β of the host, a simplified explanation of Arrhenius-plot curvature⁷ in self-diffusion experiments⁸ can be invoked. In spite of this interesting relation between the phenomena of thermal expansion

and atomic transport, measurements of $\Delta\beta_i$ are relatively rare and complicated.⁹⁻¹¹

The experimental and theoretical state of affairs for the size effect in dilute alloys, as conventionally defined, is entirely different. Even though there is a relatively larger number of measurements¹² of this quantity, there is, to date, no comprehensive theory that permits its calculation from first principles, although a number of elastic¹³⁻¹⁵ and elastic-atomic¹⁶⁻¹⁹ models have been proposed.

With regard to the experimental situation, although there are many good data for $\Delta\beta$ due to the addition of magnetic impurities to pure metals,^{20,21} there are very few precise measurements of $\Delta\beta$ in dilute, nonmagnetic alloys. The experimental problem evidently resides in the fact that for a dilute alloy (solute concentration ~ 1 at. %), $\Delta\beta/\beta \ll 1$. For example, Axon and Hume-Rothery²² found, by means of x-ray measurements on an

AlLi alloy, that $\Delta\beta > 0$, whereas Zhmudskiy's²³ data for the same alloy imply that $\Delta\beta < 0$, even though high-purity aluminum was used in both experiments. In another example, although Bailey *et al.*²⁴ measured β and $\beta + \Delta\beta$ of Pd and Pd-4 at. % Ag, respectively, to a precision of $\sim 1.5\%$, $\Delta\beta$ can be determined to no better than about 60%. Specifically, it is found at 273 K that $\beta = (11.5 \pm 0.17) \times 10^{-6} \text{ K}^{-1}$, $\beta + \Delta\beta = (11.9 \pm 0.17) \times 10^{-6} \text{ K}^{-1}$, and thus $\Delta\beta = (0.4 \pm 0.24) \times 10^{-6} \text{ K}^{-1}$. Similarly, Hume-Rothery and Boulbee's²⁵ data on Al-2.36 at. % Mg, Al-1.70 at. % Zn, and Al-1.62 at. % Cu alloys yield the following values of $\Delta\beta$: $\Delta\beta(\text{AlMg}) = (1.2 \pm 0.9) \times 10^{-6} \text{ K}^{-1}$, $\Delta\beta(\text{AlZn}) = (1.8 \pm 0.9) \times 10^{-6} \text{ K}^{-1}$, and $\Delta\beta(\text{AlCu}) = (0.6 \pm 0.9) \times 10^{-6} \text{ K}^{-1}$.

One of the rare situations in which alloy thermal-expansion data allow a determination of $\Delta\beta$ to within 5-10% involves a series of experiments on dilute AlMg alloys performed by Beaman *et al.*²⁶ From their high-temperature measurements of the temperature variation of the length and lattice parameter of the alloy, $\Delta\beta$ can be deduced to the aforementioned precision.

Given this general experimental situation, it is not too surprising that even fewer data and theories exist for the temperature variation of the size effect. In Eshelby's¹⁴ approach, a spherical cavity formed by the removal of an arbitrary number of solvent atoms is filled with a sphere consisting of the same number of solute atoms. Mechanical equilibrium and suitable boundary conditions describing the state of stress and strain at the solute-solvent interface are used to obtain the size effect as a function of the lattice parameter and elastic constants of both media. It has been recently pointed out²⁷ that the temperature derivative of Eshelby's volume change can be used to estimate $\Delta\beta$, insofar as elastic theory is valid as applied to short-range, atomic phenomena. Other less rigorous elastic models, such as those of Turner¹³ and Hughes and Brittain,¹⁵ impose arbitrary, geometrical relations between the fractional volume and fraction of cross-sectional area occupied by the solute. Although these models yield values of $\Delta\beta$ that are in limited agreement with experimental data,²⁸ it is obvious that they should be treated with extreme caution.

Semiquantitative, elastic-atomic calculations of the size effect at 0 K have been performed by Blandin and Déplante^{16,17} and Visnov *et al.*¹⁹ for a relatively large number of alloy systems. Although these studies yield interesting notions with respect to the relation between electronic and volume effects, they can not be easily exploited to calculate the temperature dependence of the size effect, namely, $\Delta\beta$.

Using the Dagen *et al.*,²⁹ pseudopotentials for

Li and Mg, Beauchamp *et al.*³⁰ derived concentration-dependent interionic potentials which they subsequently used to calculate the elastic constants of LiMg alloys at 0 K. As the interionic solute-solvent potential used is electronic-density and hence temperature dependent, it would appear that such a potential could be used to calculate the temperature dependence of another alloy property, such as the size effect.

In the present work we present the details of a series of thermal-expansion measurements on dilute AlMg and AlCa alloys for which the readily available interionic potentials of the constituents allow a model calculation of $\Delta\beta$ as well. In addition, since Mg and Ca are both divalent, this choice of solute atoms presents the possibility of experimentally confirming the importance of the solute-solvent valence difference^{16,31} in determining the changes in the properties of the host lattice induced by the solute.

Finally, the work described in this paper was undertaken to see whether at temperatures comparable to or less than the Debye temperature Θ_D of the solvent, the solute defect structure is as anharmonic as that of the thermally activated vacancy at high temperature or that of irradiation-produced defect structures¹¹ at low temperature.

II. THEORY

Ω_i consists of basically two contributions. First of all, because of the difference between the atomic volumes Ω and Ω_s of the host and solute atoms, respectively, energy is required to equalize these volumes.^{32,33} Thus, we imagine the formation of the infinitely dilute alloy in the following way. Ω_s is isothermally expanded or compressed to the final volume Ω by means of a hydrostatic pressure p given by

$$p = \int_{\Omega_s}^{\Omega} \left(\frac{\partial p}{\partial V} \right)_T dV = B_s \ln \left(\frac{\Omega_s}{\Omega} \right), \quad (1)$$

where B_s is just the isothermal bulk modulus of the solute crystal. This pressure is nothing more than the rate of change, with respect to volume, of the elastic formation energy E_1 required to accommodate the misfit, i.e.,

$$\left(\frac{\partial E_1}{\partial \Omega} \right)_T = -B_s \ln \left(\frac{\Omega_s}{\Omega} \right). \quad (2)$$

At $T = 0$ K,

$$\Omega_i = \left(\frac{\partial E^f}{\partial p} \right)_T, \quad (3)$$

where E^f is the formation energy of the infinitely dilute alloy. Even for $T \neq 0$ K, Eq. (3) is valid to a very good approximation³⁴ ($\sim 10^{-3}$). Using Eqs.

(2) and (3) to evaluate the elastic contribution Ω_{i1} to Ω_i , we obtain

$$\Omega_{i1} = \left(\frac{\partial E_1'}{\partial p} \right)_T = \left(\frac{\partial \Omega}{\partial p} \right)_T \left(\frac{\partial E_1'}{\partial \Omega} \right)_T$$

or

$$\Omega_{i1} = \Omega (B_S/B) \ln(\Omega_S/\Omega). \quad (4)$$

The second contribution Ω_{i2} to the formation volume Ω_i arises from the interatomic force changes that occur during the alloying process. This contribution is suitably handled by the lattice statics method^{34,35}:

$$\Omega_{i2} = \frac{G}{3B}, \quad (5)$$

where

$$G = \sum_{i=1}^{\infty} n_i r_i \Psi'(r_i + u_i), \quad (6)$$

and where B is, of course, the bulk modulus of the host. Here, n_l is the number of atoms in the l th shell, r_l is the distance between a host atom in the l th shell and the substitutional impurity located at the origin, and $\Psi'(r_i + u_i)$ is the first derivative of the host-impurity interaction potential evaluated at the relaxed position $r_i + u_i$ (u_i being the relaxation displacement from the normal lattice site). The interaction potential Ψ is given by¹⁸

$$\Psi = \Phi_S - \Phi, \quad (7)$$

where Φ is the interionic potential of the host lattice, and Φ_S (Ref. 36) is the interaction potential between a solute and host atom in the alloy system.

The problem of calculating the formation volume of the impurity, $\Omega_i = \Omega_{i1} + \Omega_{i2}$, thus reduces to one of calculating the dipole moment G of the impurity by means of suitable expressions for Φ and Φ_S , inasmuch as Ω_{i1} is easily evaluated by recourse to published experimental values of B_S , B , Ω_S , and Ω .

As can be seen from Eq. (6), it is necessary to evaluate the relaxation displacements u_i in order to determine G . The present approach is to calculate u_1 and u_2 by means of a Green's-function method (see Appendix A) while using $u_i = G/(4\pi \times \langle c_{11} \rangle r_i^2)$ ⁽⁴⁾ for all the higher-order displacements. As the host lattice in the present case is aluminum, the isotropic elastic expression cited above is adequate, especially when the Voigt-averaged³⁷ value of c_{11} is used. Separating Eq. (6) into a sum over first and second neighbors and another sum over all the rest, we obtain the following expression for G :

$$G = \frac{\sum_{i=1}^2 n_i r_i \Psi'(r_i + u_i) + \sum_{i=3}^{\infty} n_i r_i \Psi'(r_i)}{1 - \left(\frac{1}{12} \pi \langle c_{11} \rangle \right) \sum_{i=3}^{\infty} (n_i/r_i) \Psi''(r_i)}. \quad (8)$$

As real-space lattice sums in aluminum are known to converge rather poorly,²⁹ the numerator as well as the denominator of Eq. (8) present a formidable calculational problem. Fortunately, these sums can be evaluated by means of a modified Ewald summation technique.³⁸ Briefly, the technique is based on dividing the crystal into two regions whose frontier is defined by a particular shell ($l=n$) at which the real potential Ψ is very closely equal to its Friedel asymptotic value Ψ_{AS} , i.e., the numerator of Eq. (8) can be written as

$$\sum_{i=1}^{\infty} n_i r_i^p \Psi^{(q)}(r_i) = \sum_{i=1}^n n_i r_i^p [\Psi^{(q)}(r_i) - \Psi_{AS}^{(q)}(r_i)] + \sum_{i=1}^n n_i r_i^p \Psi_{AS}^{(q)}(r_i), \quad (9)$$

where

$$\Psi_{AS}(r) = A_1 \cos(2k_F r)/(2k_F r)^3 + A_2 \sin(2k_F r)/(2k_F r)^4, \quad (10)$$

where $\Psi_{AS}(r)$ is conveniently taken as the sum of two sinusoidal terms and k_F is the Fermi wave vector of the solvent lattice for the case of an infinitely dilute alloy.

The second term on the right-hand side of Eq. (9) can, in general, be decomposed into sums of the form $\sum_i n_i r_i^{-p} \exp(2ik_F r_i)$. The numerical values of these sums are readily available.³⁸ After A_1 and A_2 are determined by matching Ψ_{AS} , Ψ'_{AS} and Ψ''_{AS} to Ψ , Ψ' , and Ψ'' at a shell sufficiently far from the origin, Eq. (10) is substituted in Eq. (9). The two terms corresponding to $p=+1$, $q=1$, and $p=-1$, $q=2$ are then substituted in Eq. (8) in order to evaluate G .

Thus, between Eqs. (4), (5), and (8), for a potential which takes into account the variation of electronic charge density with lattice parameter²⁹ (or equivalently temperature), the temperature dependence of Ω_i can be determined.

III. EXPERIMENTAL TECHNIQUE

A. Physical basis of the measurement

For an isotropic material of volume V_0 , the volumetric coefficient of thermal expansion β is determined by measuring the temperature dependence of the specimen's length l_0 :

$$\beta = 3\alpha = 3l_0^{-1} \left(\frac{\partial l_0}{\partial T} \right)_p = V_0^{-1} \left(\frac{\partial V_0}{\partial T} \right)_p, \quad (11)$$

where α is the linear coefficient of thermal expansion.

sion. If we now simultaneously measure the temperature dependence of the length l of a specimen containing an impurity concentration and the length l_d of a pure host dummy, we obviously can write

$$\frac{l}{l(T)} \frac{dl(T)}{dT} - \frac{l}{l_d(T)} \frac{dl_d(T)}{dT} = \Delta\alpha, \quad (12)$$

where $\Delta\alpha$ is the change in the linear coefficient of thermal expansion induced by the impurity concentration. For an impurity concentration $C_i \ll 1$, it is easily shown⁷ that

$$\Delta\beta = C_i(\Omega_i/\Omega)(\beta_i - \beta) = C_i d(\Omega_i/\Omega)/dT, \quad (13)$$

where

$$\beta_i = \Omega_i^{-1} \left(\frac{\partial \Omega_i}{\partial T} \right)_p. \quad (14)$$

β_i is just the intrinsic coefficient of thermal expansion of a single impurity and $\Delta\beta = 3\Delta\alpha$. Substituting Eq. (13) into Eq. (12) and integrating with respect to temperature from T_L (lower end of the temperature range) to T_U (upper end of the temperature range), we obtain

$$\ln[l(T_U)/l(T_L)] - \ln[l_d(T_U)/l_d(T_L)] \\ = (C_i/3) [\Omega_i(T_U)/\Omega(T_U) - \Omega_i(T_L)/\Omega(T_L)]$$

or

$$\Delta l/l(T_L) - \Delta l_d/l_d(T_L) \\ \cong (C_i/3) [\Omega_i(T_U)/\Omega(T_U) - \Omega_i(T_L)/\Omega(T_L)], \quad (15)$$

where $\Delta l = l(T_U) - l(T_L) \ll l(T_L)$ for both the specimen and the dummy. Using Eq. (11), the temperature-averaged value $\langle \beta \rangle$ of β in the interval $T_L < T < T_U$ is given by

$$\exp[\langle \beta \rangle (T_U - T_L)] = \Omega(T_U)/\Omega(T_L). \quad (16)$$

Substituting Eq. (16) in Eq. (15) yields

$$\Delta l/l(T_L) - \Delta l_d/l_d(T_L) \cong (C_i/3) \Omega_i(T_U)/\Omega(T_U) \\ \times \{1 - \exp[-\langle \beta_i - \beta \rangle (T_U - T_L)]\}. \quad (17)$$

Thus, in order to determine $\langle \beta_i \rangle$, we need to have the values of β , C_i , and $\Omega_i(T_U)/\Omega(T_U)$, as well as the measurements of Δl and Δl_d . The size effect Ω_i/Ω is typically measured by means of x rays: $\Omega_i/\Omega = (3/C_i)(\Delta a/a_0)_{C_i}$, where $(\Delta a/a_0)_{C_i}$ is the fractional change in the host lattice parameter a_0 due to the impurity concentration C_i . Thus, Eq. (17) can be written as

$$\Delta l/l(T_L) - \Delta l_d/l_d(T_L) \\ \cong (\Delta a/a_0)_{C_i} \{1 - \exp[-\langle \beta_i - \beta \rangle (T_U - T_L)]\}. \quad (18)$$

The choice of the experimental method of mea-

suring $\langle \beta_i - \beta \rangle$ is obviously a sensitive function of the order of magnitude of the quantity $\Delta l - \Delta l_d$. Inasmuch as $\Delta l - \Delta l_d \cong l(T_L)(T_U - T_L)\Delta\beta/3$, the problem of estimating $\Delta l - \Delta l_d$ is equivalently that of estimating $\Delta\beta$. The high-temperature measurements ($523 \text{ K} \leq T \leq 773 \text{ K}$) of Beaman *et al.*²⁶ on dilute AlMg alloys yield $\Delta\beta/C_i \approx 2 \times 10^{-5} \text{ K}^{-1}$, whereas those of Afanas'yev *et al.*³⁹ ($293 \text{ K} \leq T \leq 723 \text{ K}$) yield $\Delta\beta/C_i \sim 10^{-4} \text{ K}^{-1}$. Furthermore, the excellent low-temperature ($4 \text{ K} \leq T \leq 25 \text{ K}$) data of Khan and Griffiths²¹ for CuMn and AgMn alloys indicate $\Delta\beta/C_i \approx 10^{-5} \text{ K}^{-1}$. If we take $\Delta\beta/C_i \sim 3 \times 10^{-5} \text{ K}^{-1}$, $\Delta l - \Delta l_d \sim 0.5 \text{ } \mu\text{m}$ for $C_i \sim 10^{-2}$ (atomic fraction), $l(T_L) \sim 5 \text{ cm}$, and $T_U - T_L \sim 100 \text{ K}$. As can be seen in Appendix B, measuring the differential length change $\Delta l - \Delta l_d = 0.5 \text{ } \mu\text{m}$, with an uncertainty of $\pm 3 \times 10^{-2}$, results in an overall uncertainty in $\langle \beta_i \rangle$ of about 10%. The only way to obtain this kind of precision without recourse to complicated calibration procedures is to utilize an optical technique. A specially designed Fabry-Perot differential interferometer was decided upon, as explained in the following section.

B. Apparatus

1. Interferometric cell

For $l(T_L) \cong l_d(T_L) \sim 5 \text{ cm}$ and $|l(T_L) - l_d(T_L)| < 5 \text{ } \mu\text{m}$, $l(T_L)$ and $l_d(T_L)$ can be considered equal in Eq. (18) without introducing more than a 3% error in $\langle \beta_i \rangle$ (see Appendix C). Under these conditions we can write Eq. (18) as

$$[\Delta l(T) - \Delta l_d(T)]/l(T_L) \\ \cong (\Delta a/a_0)_{C_i} \{1 - \exp[-\langle \beta_i - \beta \rangle (T - T_L)]\}. \quad (19)$$

The quantity $\Delta l(T) - \Delta l_d(T)$ appearing above can be directly measured by attaching optical surfaces to both the specimen and dummy in such a way that the displacement of the fringe pattern resulting from the incidence of monochromatic light on the optical surfaces is proportional to the quantity $\Delta l(T) - \Delta l_d(T)$. Specifically, the essential aspects of the specimen-dummy optical-surfaces configuration are indicated in Fig. 1. The surface S_1 of the upper optical quartz disk partially transmits the normally incident He-Ne laser beam ($\lambda = 6328 \text{ } \text{Å}$) that is subsequently almost entirely reflected by the surface S_2 of the lower quartz disk. Under these conditions it is easily shown⁴⁰ that the optical wedge formed by S_1 and S_2 gives rise to a linear fringe pattern described by the relation $e_n = (2n + 1)\lambda/4$. λ is the wavelength of the incident light and n is a whole number defining the particular dark fringe found at those points for which the separation of S_1 and S_2 is equal to e_n . When the surface S_1 is translated parallel to itself by a

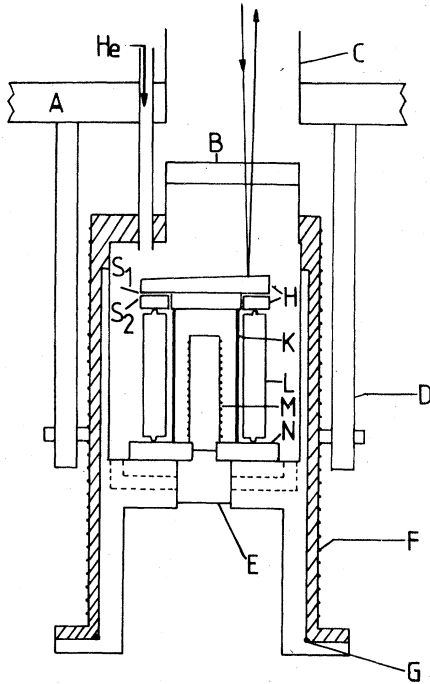


FIG. 1. Configuration of the specimen, dummy, optical elements, and experimental chamber. A—flange, B—optical port, C—stainless-steel tube, D—supporting columns, E—electrical feed-through, F—electric main heater, G—indium seal, H—quartz optical interference wedges, K—aluminum alloy specimen, L—aluminum dummy, M—small electric heater, N—aluminum supporting disk.

distance ΔS , each fringe translates parallel to itself by a corresponding distance $\Delta H = (2i/\lambda)\Delta S$,⁴⁰ where i is the interfringe distance. Two remarks are in order. First, ΔS can be set equal to $\Delta l(T) - \Delta l_d(T)$, provided that the average separation between S_1 and S_2 is no greater than about $50 \mu\text{m}$. In this case, the thermal expansion associated with this thickness of quartz makes ΔS equal to $\Delta l(T) - \Delta l_d(T)$ to within better than 1% (see Appendix D). Second, as $\Delta S = (\lambda/2i)\Delta H$, the precision with which $\Delta l(T) - \Delta l_d(T)$ is measured obviously depends on the precision with which i and ΔH are in turn measured. This evidently necessitates fringes of small half-width with respect to i . Reflectivities of nearly 100% and 90% of S_1 and S_2 , respectively, result in a half-width to interfringe ratio of $\sim 10^{-2}$. This allows a precision of $\sim 10^{-2}$ in the measurement of the fringe-system displacement.

As can be seen from Fig. 1, the light tubular specimen is concentrically surrounded by a relatively massive dummy. This geometry tends to minimize the variation in the difference between the temperature of the dummy and specimen, ΔT_{SD} , in the range $T_L < T < T_U$. It is shown in Appendix

E that $\Delta T_{SD} = 50 \text{ mK}$ introduces an uncertainty of about 10% in $\langle \beta_i \rangle$ for a dummy-specimen temperature excursion of $\sim 100 \text{ K}$. In fact, as verified by measurements with a differential thermocouple, ΔT_{SD} never exceeded 25 mK.

As shown in Fig. 2, the specimen and dummy are supported by an optically flat aluminum disk situated at the bottom of the inner chamber. A small electric heater, mounted on the axis of this disk and activated momentarily after each run, provides a means of correlating the sign of $\Delta \beta$ with the fringe-system displacement.

The temperature was controlled and measured by means of detectors in contact with the dummy. A Thor Cryogenics Mark-II temperature controller permitted fluctuations of no greater than 10 mK about each set point. Electrical communication between the optical cell and external instruments was effected by means of a vacuum electrical feed-through seal assembly located just below the supporting disk.

As can be seen in Fig. 2, the inner part of the specimen chamber, which houses the optical cell, is surrounded by a concentric, coverlike structural element that contains the optical port and the main electrical heating element. The excellent contact between the external surface of the inner chamber and the internal surface of the outer envelope makes possible the creation of a vacuum seal with an indium O ring located at the internal corner of the lower flange.

2. Fringe acquisition and counting system

As schematically shown in Fig. 2, a highly reflecting right-angle prism guides the initially horizontal laser beam to the optical cell located about a meter below the supporting table. After producing the interference fringes in the optical wedge, the beam is redeviated by the same right-angle prism so that its final orientation is horizontal. The

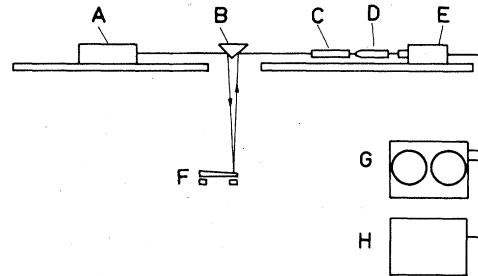


FIG. 2. Block diagram of the optical circuit and fringe recording system. A—laser, B—prism, C—telescope, D—microscope, E—TV camera, F—optical wedges, G—video tape recorder, H—TV screen.

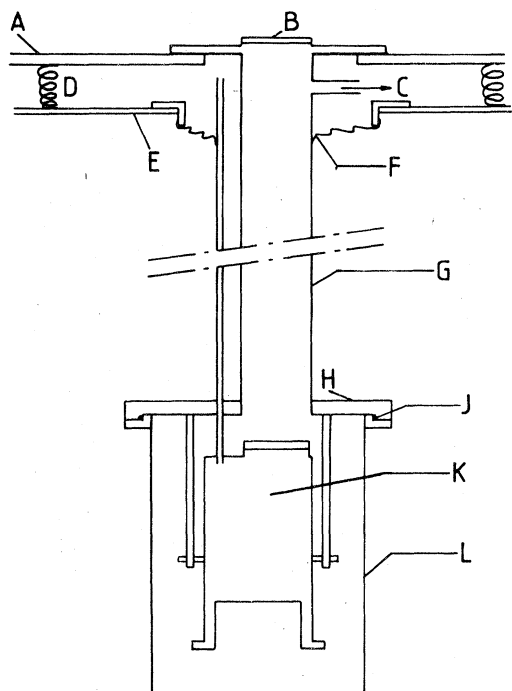


FIG. 3. Mechanical assembly. A—supporting slab, B—optical port, C—vacuum, D—antivibration pads, E—upper surface of glove box, F—soft airtight coupling, G—stainless-steel tube, H—flange, J—indium seal, K—inner chamber, L—outer envelope.

image of the interference fringes is then relayed by a telescope to a microscope whose optical output can then be viewed in a variety of ways.

It is evident that a basic factor in measuring the displacement of the fringe system is the knowledge of the number of times that the fringe system periodically assumes its initial position during a run. Suffice it to say that this ambiguity in the fringe-system position can be removed in a number of ways.^{41,42} In the present experiment we use the novel technique of recording the fringes on videotape by means of a closed-circuit television camera that views the optical output of the microscope. Since a typical run lasts about two weeks, the position of the fringe system is recorded in slow motion so that playback at normal speed takes no more than about 10 hours. The fringe-system image is simultaneously displayed on a television screen so that the progress of each run can be easily monitored.

3. Mechanical assembly

Figure 3 indicates that the experimental chamber is attached to a stainless steel connecting tube which is in turn anchored to a stainless steel slab

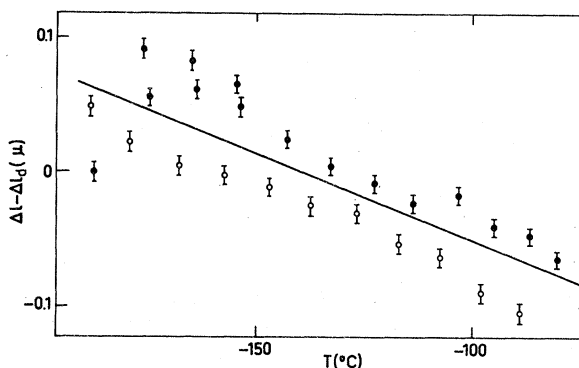


FIG. 4. $\Delta l - \Delta l_d$ vs T for Al-0.064 at.% Ca.

that supports the optical system (laser, prism, telescope, microscope, and television camera). The experimental chamber consists of two parts: an inner copper chamber housing the optical cell and an outer stainless steel chamber that is immersed in liquid nitrogen. The space between these two chambers is evacuated so that the temperature of the specimen can be controlled with relatively small amounts of electrical energy (~ 50 W).

It can be seen in Fig. 3 that the supporting slab is mounted on the upper surface of a rather large glove box (volume ~ 3 m³). The antivibration pads that couple the massive supporting slab to the glove box prevent irreversible changes in optical-cell geometry as well as reversible oscillations that can degrade the quality of the fringe-system image.

The glove box is also extremely useful in providing a dry atmosphere that prevents the formation of ice buildups that would mechanically couple the liquid nitrogen dewar to the stainless steel connecting tube, and hence to the optical cell.

C. Experimental procedure

1. Specimen preparation

The specimens and dummy were machined from bar stock furnished by Pechiney, France. The 99.99%-pure aluminum was used for the dummy as well as for the starting material for the AlCa and AlMg alloys.

At every stage of the machining operations used to fabricate the dummy and specimens, an electronic dial gauge having a sensitivity of $0.2 \mu\text{m}$ was used to insure that the length of each specimen never differed by more than $5 \mu\text{m}$ from the length of the dummy. In addition, the optical planes defined by the upper feet of a specimen-dummy pair were always parallel to better than 5×10^{-4} rad ($i \sim 1$ mm).

After machining, the specimens were chemically cleaned before annealing in air at $\sim 300^\circ\text{C}$ during ~ 15 h. The oxide that forms during the anneal prevents the evaporative loss of Mg and Ca, both of which are relatively volatile when dissolved in Al.

2. Measurements

a. Differential thermal expansion. Specimens were mounted in the experimental chamber at room temperature. After centering the dummy on the supporting disk (see Fig. 1), a specially designed jig was used to lower the specimen into the dummy without deforming its extremely fragile feet. As the jig permits a specimen-dummy concentricity of ~ 0.5 mm, unwanted specimen-dummy mechanical contact was avoided.

After positioning the optical wedges on the specimen and dummy, a microscope slide containing a grid of pyramidal, diamond indentations was carefully placed on the upper surface of the upper optical wedge in such a way as to intercept the laser beam. The grid spacing was chosen so that the image of at least one of the indentations always appeared superimposed on the image of the fringes. The only physically significant displacement of the fringe system is one that is measured with respect to an indentation: Any change in the thermal stresses acting on the long tube connecting the sample chamber to the supporting slab can change the orientation of the laser beam with respect to the optical wedges. This has the unwanted effect of producing an apparent displacement of the fringe system even when the distance between S_1 and S_2 does not necessarily change.

The inner and outer parts of the specimen chamber were brought in contact by means of a precision jack in order to avoid excessive vibrations that would dislodge the optical wedges from the specimen and dummy. The entire system was then pumped down to a pressure of $\sim 10^{-2}$ Torr before filling the optical cell with helium. The good thermal conductivity of helium helps to minimize ΔT_{SD} . The system was then submerged in liquid nitrogen, slowly cooling to ~ 80 K for 12–15 hours.

After adjusting the geometry of the various optical paths so that sharp images of the fringe system and the fiducial markers are obtained on the television screen, the temperature of the optical cell was increased in a stepwise fashion from ~ 80 –180 K. The optical cell was periodically brought into thermal equilibrium at ~ 10 -K intervals so that a statistically significant number of fringe-system positions could be measured in the temperature range considered. A "cooling" run was always effected after each "heating" run so that deviations

from thermal equilibrium as well as mechanical hysteresis could be evaluated. The fringe-system position as well as the interfringe distance were measured only when temperature fluctuations stayed within 10-mK limits during ~ 2 h prior to the measurements. Distance measurements were made directly on the television screen with an ordinary ruler to ± 1 mm. This uncertainty is equivalent to an uncertainty of $\pm 4 \times 10^{-3}$ μm in the actual distances, inasmuch as interfringe distances were typically ~ 80 mm, as seen on the television screen employed.

After each run, the lengths of the dummy and specimen were remeasured so that any possible permanent deformations could be evaluated: differences in length never exceeded 4 μm .

b. X-ray lattice parameter measurements. The size effect, $(3/C_i)(\Delta a/a_0)_{C_i}$, was determined by means of the Laue back-reflected x rays that sampled the well-annealed surfaces of the alloys studied: AlCa at calcium concentrations of 0.060 and 0.081 at. %, and AlMg at magnesium concentrations of 0.115 and 1.065 at. %.

The 2 mm thick square specimens were mounted in a Philips goniometer which allowed an uncertainty of $\pm 10^{-4}$ \AA in the lattice-parameter measurement. This gives rise to an uncertainty of between 3 and 70% in the size effect (see Appendix F).

Both x-ray and thermal-expansion specimens were chemically analyzed at the end of each run so that precise estimations of the alloy compositions could be ascertained.

IV. RESULTS

A. Experiment

1. Differential thermal-expansion measurements and the determination of $\Delta\beta/C_i$

The measured values of $\Delta l - \Delta l_d$ as a function of temperature are shown in Figs. 4, 5, 6, and 7 for

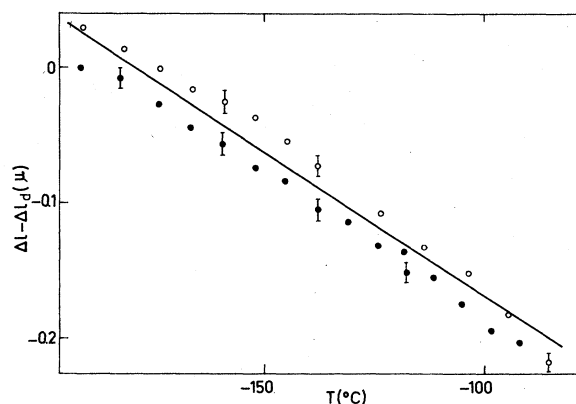
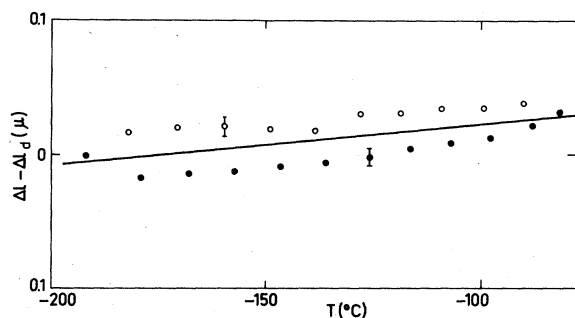
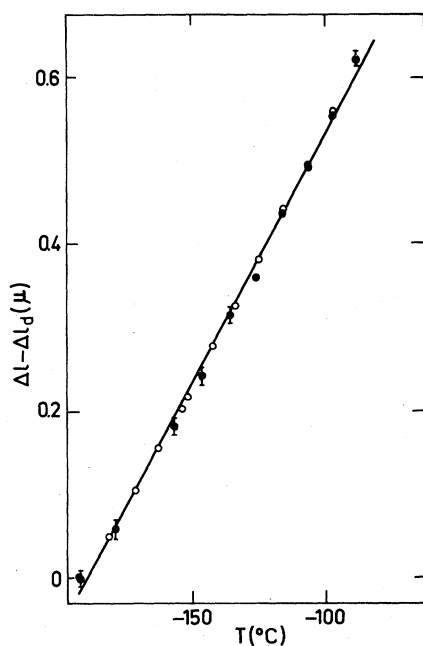
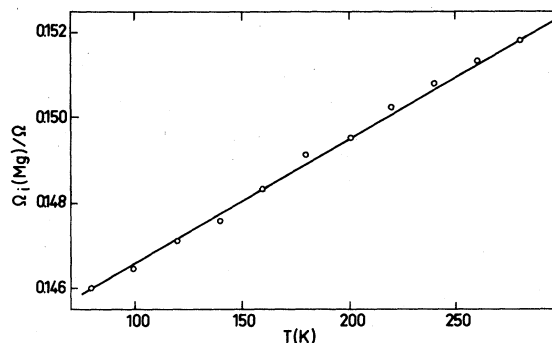


FIG. 5. $\Delta l - \Delta l_d$ vs T for Al-0.090 at. % Ca.

FIG. 6. $\Delta l - \Delta l_d$ vs T for Al-0.115 at. % Mg.

the four alloys studied. It can be seen from these graphs that $\Delta l - \Delta l_d$, to within the experimental precision, varies linearly with the temperature. Thus, according to Eq. (17), the slopes of the best-fit lines to these data, together with the nominal dummy or specimen length, allow the determination of $\Delta\beta$. As can be seen from Table I, the values of $\Delta\alpha$ calculated from the heating-run and the cooling-run data are the same to within the experimental uncertainty. This uncertainty varies from about $\pm 20\%$ for the most dilute alloys to about $\pm 2\%$ for the Al-1.065-at. % Mg alloy.

Although the "heating" and "cooling" slopes are the same to within the experimental precision, we notice that only in the case of the Al-1.065-at. % Mg alloy is there a complete absence of the hysteresis that appears to be associated with the

FIG. 7. $\Delta l - \Delta l_d$ vs T for Al-1.065 at. % Mg.FIG. 8. Calculated temperature dependence of Ω_i (Mg)/ Ω .

other measurements of $\Delta l - \Delta l_d$ with temperature. The amplitude of the hysteresis loop increases with decreasing impurity concentration, attaining a maximum value of $0.11 \mu\text{m}$ in the "zero-effect" measurement that was performed on a pure-aluminum specimen. As we attribute this hysteresis to the irreversible plastic deformation of the specimen feet, it is not too surprising that increasing the impurity concentration, and hence, the specimen's yield point, increases the overlap between the "heating" and "cooling" data. Inasmuch as there is thus a lack of superposition between the actual and "zero-effect" measurements, the latter can not be used to correct the former.

It should be noted that $\Delta\beta$ (AlMg) > 0 , whereas $\Delta\beta$ (AlCa) < 0 . It can be observed from Table II that $\Delta\beta/C_i$ varies with C_i for both types of alloys considered. This dependence is less marked in the case of AlCa, inasmuch as the change in $\Delta\beta/C_i$ with concentration is comparable to its experimental uncertainty. The arithmetic average of the two values indicated in Table II is thus $\Delta\beta$ (Ca)/ $C_i = -(13.2 \pm 0.2) \times 10^{-5} \text{ K}^{-1}$. On the other hand, $\Delta\beta/C_i$ unambiguously increases with C_i in AlMg: $\Delta\beta$ (Mg)/ $C_i = (1.8 + 0.6) \times 10^{-5} \text{ K}^{-1}$ for C_i (Mg) = 0.115 at. % and $\Delta\beta$ (Mg)/ $C_i = (3.33 \pm 0.12) \times 10^{-5} \text{ K}^{-1}$ for C_i (Mg) = 1.065 at. %.

We also point out that to within the experimental uncertainty there is no detectable variation with temperature of the slope of the graph of $\Delta l - \Delta l_d$ vs T for each of the alloys studied. This means that although β more than doubles in the temperature range explored, $\Delta\beta$ (Mg)/ C_i and $\Delta\beta$ (Ca)/ C_i are relatively temperature independent.

2. Impurity-intrinsic coefficient of thermal expansion, β_i

In order to determine the value of $\langle\beta_i\rangle/\langle\beta\rangle$ for both Mg and Ca dissolved in Al, the experimental values of $\Delta\beta$ and the size effect, $(3/C_i)(\Delta a/a_0)c_i$, are injected into Eq. (19).

TABLE I. Best-fit slopes of $\Delta l - \Delta l_d$ vs T.

Alloy	$\Delta\alpha$ (K ⁻¹)		
	Heating run	Cooling run	Both runs together
Al-0.060 at. % Ca	$-(0.24 \pm 0.04) \times 10^{-7}$	$-(0.27 \pm 0.014) \times 10^{-7}$	$-(0.25 \pm 0.04) \times 10^{-7}$
Al-0.081 at. % Ca	$-(0.42 \pm 0.01) \times 10^{-7}$	$-(0.44 \pm 0.01) \times 10^{-7}$	$-(0.44 \pm 0.02) \times 10^{-7}$
Al-0.115 at. % Mg	$+(0.07 \pm 0.014) \times 10^{-7}$	$+(0.046 \pm 0.007) \times 10^{-7}$	$+(0.06 \pm 0.02) \times 10^{-7}$
Al-1.065 at. % Mg	$+(1.20 \pm 0.022) \times 10^{-7}$	$+(1.20 \pm 0.016) \times 10^{-7}$	$+(1.18 \pm 0.013) \times 10^{-7}$

As can be seen from Table III, the size effect is relatively constant in the case of Ca, whereas it increases significantly with increasing impurity concentration in the case of Mg. As the experimental uncertainty in the size effect is about $\pm 25\%$ for the AlCa alloys, and $\pm 75\%$ and $\pm 5\%$ for the low- and high-concentration AlMg alloys, respectively, an expression which linearizes Eq. (19) for $\langle\beta_i - \beta\rangle(T_U - T_L) \ll 1$ is entirely justified. Taking $\langle\beta\rangle = 45 \times 10^{-6} \text{ K}^{-1}$ between -190 and -90°C , the linearized form of Eq. (19) yields the values of $\langle\beta_i\rangle/\langle\beta\rangle$ indicated in Table II. In spite of the large uncertainties ($\pm 40\%$) in the values of $\langle\beta_i\rangle/\langle\beta\rangle$ for all except the most concentrated AlMg alloy, we see that the intrinsic coefficient of thermal expansion of both the Mg and Ca impurities are \sim three times larger than that of the lattice. However, $\beta_i(\text{Mg}) > 0$, whereas $\beta_i(\text{Ca}) < 0$.

It should be noted that in the case of the Al-0.115 at. % Mg alloy, the size-effect data of Poole and Axon,⁴³ being more precise than ours, were used to calculate $\langle\beta_i\rangle/\langle\beta\rangle$.

B. Present calculation

The calculated variation of $\Omega_i(\text{Mg})/\Omega$ with temperature is shown in Fig. 8. Between 80 and 300 K, $\Omega_i(\text{Mg})/\Omega$ varies linearly with temperature in the range $0.146 \leq \Omega_i(\text{Mg})/\Omega \leq 0.152$. From Eq. (13), $\Delta\beta/C_i = d(\Omega_i/\Omega)/dT$. A best-fit straight line of $\Omega_i(\text{Mg})/\Omega$ vs T yields $\Delta\beta/C_i = (2.9 \pm 0.1) \times 10^{-5} \text{ K}^{-1}$.

The contribution of $\Omega_{i1}(\text{Mg})/\Omega$ to $\Omega_i(\text{Mg})/\Omega$ is extremely small: $-7.0 \times 10^{-3} \leq \Omega_{i1}(\text{Mg})/\Omega \leq 7.6 \times 10^{-3}$ between 80 and 300 K. Thus, in the case of Mg substitutionally dissolved in Al, the change in the interatomic force constants on alloying has little effect on the formation volume of the defect: About 95% of the formation volume has its origin in the elastic-energy change E_1^f associated with the misfit between $\Omega_s(\text{Mg})$ and $\Omega(\text{Al})$. From Eq. (12), together with the calculated values of $\Omega_i(\text{Mg})/\Omega$ vs T, we can calculate $\langle\beta_i(\text{Mg})\rangle$ and $\langle\beta_i(\text{Mg})\rangle/\langle\beta\rangle$ in the temperature range 80 to 180 K. Specifically, $\langle\beta_i(\text{Mg})\rangle = 2.4 \times 10^{-4} \text{ K}^{-1}$ and $\langle\beta_i(\text{Mg})\rangle/\langle\beta\rangle = 5.2$.

For AlCa, the calculated variation of $\Omega_{i2}(\text{Ca})/\Omega$ with temperature is shown in Fig. 9. In contrast to Mg, the temperature variation of only the atomic contribution to the total formation volume can be calculated due to the lack of experimental data for $B_{\text{Ca}}(T)$ at all temperatures except $T=300 \text{ K}$.⁴³ Using the appropriate data for Ca and Al, Eq. (4) yields $[\Omega_{i1}(\text{Ca})/\Omega]_{300 \text{ K}} = 0.26$. As reference to Fig. 9 shows that $0.286 \leq \Omega_{i2}(\text{Ca})/\Omega \leq 0.277$ between 80 and 300 K, it is obvious that in AlCa, the elastic and atomic contributions to the defect formation volume are about the same. The sum of the two contributions at 300 K yields $[\Omega_i(\text{Ca})/\Omega]_{300 \text{ K}} = 0.54$.

It should be pointed out that the utilization of isothermal elastic constants in all of the calculated results is extremely important in aluminum alloys: for Al, the isothermal bulk-modulus tem-

TABLE II. Measured values of $\Delta\beta/C_i$, $\langle\beta_i\rangle$, and $\langle\beta_i\rangle/\langle\beta\rangle$.

Alloy	$\Delta\beta/C_i$ (K ⁻¹ at. fraction ⁻¹)	$\langle\beta_i\rangle$ (K ⁻¹)	$\langle\beta_i\rangle/\langle\beta\rangle$
Al-0.060 at. % Ca	$-(11.7 \pm 2.1) \times 10^{-5}$	$-(1.3 \pm 0.6) \times 10^{-4}$	$-(2.9 \pm 1.5)$
Al-0.081 at. % Ca	$-(14.7 \pm 0.9) \times 10^{-5}$	$-(2.2 \pm 0.6) \times 10^{-4}$	$-(4.8 \pm 1.3)$
Al-0.115 at. % Mg	$+(1.8 \pm 0.6) \times 10^{-5}$	$+(2.7 \pm 1.2) \times 10^{-4}$	$+(6.0 \pm 2.7)$
Al-1.065 at. % Mg	$+(3.33 \pm 0.12) \times 10^{-5}$	$+(1.48 \pm 0.04) \times 10^{-4}$	$+(3.28 \pm 0.09)$

TABLE III. Concentration dependence of alloy lattice parameters and size effects.

Alloy	C_i (at. %)	a (Å)	$(3/C_i)(\Delta a/a)c_i$
Al pure		4.0488 ± 0.0001	
Al-Ca	0.060 ± 0.001	4.0494 ± 0.0001	0.75 ± 0.20
Al-Ca	0.081 ± 0.001	4.0495 ± 0.0001	0.65 ± 0.15
Al-Mg	0.115 ± 0.002	4.0490 ± 0.0001	0.13 ± 0.09
Al-Mg	1.065 ± 0.021	4.0535 ± 0.0001	0.36 ± 0.02

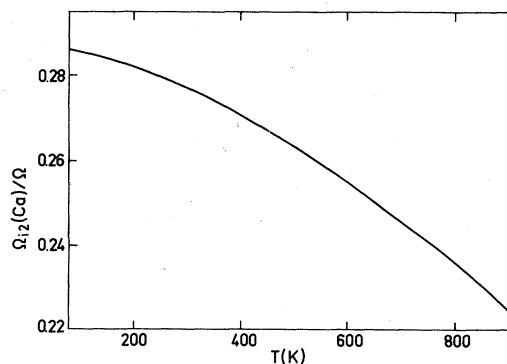
perature derivatives are typically twice as large as the isentropic ones. This factor of 2 is sufficient to change the order of magnitude as well as the sign of the impurity-intrinsic coefficient of thermal expansion.

V. DISCUSSION OF RESULTS

A. Size effect at room temperature

The fact that the size effect, in the case of AlCa, is independent of the calcium concentration to within the experimental precision, would tend to indicate that for C_i (Ca) ≤ 0.09 at. %, Ca-Ca interactions appear to play a minor role in determining the lattice distortions induced by the presence of the solute. On the other hand, there is a very marked difference between the AlMg size effects corresponding to the two concentrations studied. It is clear that for C_i (Mg) $\cong 1$ at. %, Mg-Mg interactions contribute significantly to the solute-induced lattice distortion. Evidently, due to the lack of sufficient data, it is not possible to estimate the importance of the solute-solute interaction at C_i (Mg) = 0.115 at. %.

To the knowledge of the authors, there has been no previous measurement of the size effect in dilute AlCa alloys. For AlMg the situation is entirely different. Consider the size-effect data of

FIG. 9. Calculated temperature dependence of $\Omega_{12}(Ca)/\Omega$.

previous experiments and those of the present study that appear in Table IV. As the experimental uncertainties associated with the size effect were not explicitly determined in the previous experiments that are currently cited, the uncertainties that appear in Table IV have been estimated by the present authors, and are considered to be reasonable within the context of the experimental techniques utilized. We note that the present data are in excellent agreement with those of Poole and Axon.⁴⁴ Although Rothery and Boulbee²⁵ measured the size effect in AlMg at C_i (Mg) = 2.36 at. %, the better than order-of-magnitude agreement between their value and ours for which C_i (Mg) = 1.065 at. %, is nevertheless encouraging. Returning to the data of Poole and Axon, we notice that between the concentrations of 0.18 and 0.32 at. %, the size-effect jumps from 0.16 ± 0.02 to 0.24 ± 0.02 , and then increases slowly to 0.30 ± 0.02 for C_i (Mg) = 1.93 at. %. This type of behavior is certainly consistent with the presence of solute-solute interactions for C_i (Mg) ≥ 0.18 at. %. The present experimental data confirm these tendencies.

TABLE IV. Summary of experimental data for the size effect in AlMg alloys.

C_i (at. %)	$(3/C_i)(\Delta a/a)c_i$	Remarks
0.18	0.157 ± 0.021	
0.32	0.240 ± 0.021	Measurements of Poole and Axon (Ref. 44)
0.62	0.267 ± 0.021	at 25°C.
1.28	0.279 ± 0.021	
1.93	0.297 ± 0.021	
2.36	0.225 ± 0.021	Hume-Rothery and Boulbee (Ref. 25). Measurements at 25°C.
0.115 ± 0.002	0.12 ± 0.09	Present measurements
1.065 ± 0.021	0.36 ± 0.02	at 21°C.

B. Comparison of the present data for $\Delta\beta/C_i$ with those of previous experiments

As has already been indicated, this comparison is impossible for $\Delta\beta$ (Ca)/ C_i due to a total lack of thermal-expansion data for AlCa alloys. On the other hand, the x-ray data of Hume-Rothery and Boulton²⁵ for pure aluminum and an Al-2.36-at. % Mg alloy in the temperature range from -50 to +25°C yield the following temperature-averaged coefficients of thermal expansion: $\beta = (66.9 \pm 0.6) \times 10^{-6} \text{ K}^{-1}$ and $\beta + \Delta\beta = (68.1 \pm 0.6) \times 10^{-6} \text{ K}^{-1}$. Thus, we extract from these data $\Delta\beta$ (Mg)/ $C_i = (51 \pm 36) \times 10^{-6} \text{ K}^{-1}$. From the present experimental data, $\Delta\beta$ (Mg)/ $C_i = (33.3 \pm 1.2) \times 10^{-6} \text{ K}^{-1}$ between -190 and -90°C for C_i (Mg) = 1.065 at. %. Taking into consideration the difference in alloy composition as well as the temperature range of measurement, the difference between the above values of $\Delta\beta/C_i$ nevertheless lies within the limits of uncertainty in each of the quantities.

The x-ray measurements of Beaman *et al.*²⁶ on Al-1.11-at. % Mg in the temperature range from 250 to 500°C yield $\Delta\beta/C_i = (54 \pm 3) \times 10^{-6} \text{ K}^{-1}$. This is well above the currently measured, low-temperature value of $\Delta\beta/C_i = (33.3 \pm 1.2) \times 10^{-6} \text{ K}^{-1}$ obtained for C_i (Mg) = 1.065 at. %. The apparent decrease of $\Delta\beta/C_i$ with decreasing temperature is not too surprising, inasmuch as Ω_i as well as Ω become increasingly independent of temperature as $T \rightarrow 0$, consistent with the third law of thermodynamics.

With regard to previous, less precise measurements on other dilute, substitutional alloys, the currently measured values of $\Delta\beta$ (AlMg)/ $C_i = (3.33 \pm 0.12) \times 10^{-5} \text{ K}^{-1}$ and $\Delta\beta$ (AlCa)/ $C_i = (13.2 \pm 0.2) \times 10^{-5} \text{ K}^{-1}$ are in an order-of-magnitude agreement with $\Delta\beta$ (PdAg)/ $C_i = (1 \pm 0.6) \times 10^{-5} \text{ K}^{-1}$ of Bailey *et al.*,²⁴ and $\Delta\beta$ (AlZn)/ $C_i = (10 \pm 5) \times 10^{-5} \text{ K}^{-1}$ and $\Delta\beta$ (AlCu)/ $C_i = (4 \pm 6) \times 10^{-5} \text{ K}^{-1}$ of Hume-Rothery and Boulton.²⁵

C. Comparison of currently measured values of β_i with those of point defects

For both AlMg and AlCa we note that the absolute value of the ratio $\langle\beta_i\rangle/\langle\beta\rangle$ is considerably greater than unity. This result is consistent with the high-temperature, vacancy-diffusion measurements in zinc⁹ and cadmium¹⁰ as well as the very recent low-temperature measurements on radiation-produced point-defect structures in aluminum.¹¹ In the high-pressure, self-diffusion experiments referred to, the activated vacancy is found to have a coefficient of thermal expansion some fifteen times larger than that of the perfect lattice. In the latter measurement on irradiated aluminum it is found that the coefficient of thermal expansion

of the neutron-produced Frenkel defects (isolated vacancies and small interstitial clusters) is 12 times larger than that of the pure metal. In light of the present measurements it would appear that both intrinsic defects and impurities are endowed with intrinsic coefficients of thermal expansion that are substantially larger than that of the perfect lattice ($|\beta_{i,v}|/\beta \sim 4-15$), even in the "reduced-temperature" range $0.2 < T/\Theta_D < 0.4$.

It should be emphasized that β_i can be either positive or negative. In the present experiment β_i (Mg) > 0 , whereas β_i (Ca) < 0 : magnesium increases the aluminum-lattice anharmonicity, whereas calcium decreases it. The fact that Mg and Ca are both divalent would then tend to indicate that the solute-solvent valence difference plays a role less important than previously thought^{16, 31} in determining solute-induced changes in host-lattice properties. At least, thermal expansion would appear to be independent of valence effects for the two aluminum alloys considered. Complementary measurements are obviously required to validate the universality of these limited results.

D. Present calculation

1. Size effect

The calculated value of Ω_i (Mg)/ Ω at 300 K is 0.152, as compared to the x-ray measured values of 0.129 ± 0.092 and 0.360 ± 0.018 at magnesium concentrations of 0.115 and 1.065 at. %, respectively. As has been stated earlier, the fact that the measured defect volume varies with the defect concentration indicates that Mg-Mg interactions are important at C_i (Mg) = 1.065 at. %. As the present calculation of Ω_i (Mg)/ Ω assumes that the alloy is infinitely dilute, the calculated value should logically be compared with the experimental value measured at the smallest magnesium concentration (0.115 at. %). At this concentration, the agreement is good: $[\Omega_i$ (Mg)/ $\Omega]^{theor} = 0.152$, whereas $[\Omega_i$ (Mg)/ $\Omega]^{meas} = 0.130 \pm 0.09$.

The calculated value of the size effect for calcium at 300 K, $[\Omega_i$ (Ca)/ $\Omega]_{300 \text{ K}} = 0.54$, is in good agreement with the currently measured value of 0.70 ± 0.18 . In contrast to AlMg, both the calculated and measured size effects in AlCa correspond to infinite dilution of the alloy.

2. Impurity-induced thermal expansion change, $\Delta\beta/C_i$

a. Currently measured and calculated values.

Eq. (16) allows us to calculate $\Delta\beta/C_i$ by determining the slope of the calculated graph of Ω_i (Mg)/ Ω vs T . The slope of the graph of Fig. 8 yields $\Delta\beta/C_i = 2.9 \times 10^{-5} \text{ K}^{-1}$, whereas Table II gives the

measured values of $(1.8 \pm 0.6) \times 10^{-5} \text{ K}^{-1}$ and $(3.33 \pm 0.12) \times 10^{-5} \text{ K}^{-1}$ corresponding to magnesium concentrations of 0.115 and 1.065 at. %, respectively. The currently calculated value of $\Delta\beta/C_i$ is obviously in good agreement with the measured values inasmuch as it falls between them.

For calcium, reference to Table II shows that the measured values of $\Delta\beta/C_i$ are $-(11.7 \pm 2.1) \times 10^{-5} \text{ K}^{-1}$ and $-(14.7 \pm 0.9) \times 10^{-5} \text{ K}^{-1}$ corresponding to calcium concentrations of 0.060 and 0.081 at. %, respectively. The arithmetic average of these data yields $\Delta\beta/C_i = -(13 \pm 2) \times 10^{-5} \text{ K}^{-1}$. As $\Delta\beta/C_i = d(\Omega_i/\Omega)/dT$, the absence of experimentally measured temperature derivatives of the elastic constants prohibits a calculation of $\Delta\beta(\text{Ca})/C_i$. However, we can use the experimentally measured value of $\Delta\beta/C_i$ to roughly estimate the value of $(B_{\text{Ca}}^{-1} dB_{\text{Ca}}/dT)_T$. From the experimental data in the range from 80 to 190 K, $d(\Omega_i/\Omega)/dT = \Delta\beta/C_i = -(13 \pm 2) \times 10^{-5} \text{ K}^{-1}$. We suppose that $d(\Omega_i/\Omega)/dT$ maintains this value to 300 K. From the best-fit parabola to Ω_{i2}/Ω vs T (see Fig. 9), we find that $[d(\Omega_{i2}/\Omega)/dT]_{300 \text{ K}} = -5.8 \times 10^{-5} \text{ K}^{-1}$. Thus, the "elastic derivative" $[d(\Omega_{i1}/\Omega)/dT]_{300 \text{ K}} = -(7 \pm 2) \times 10^{-5} \text{ K}^{-1}$. Using Eq. (4) and our calculated room-temperature value of Ω_{i1}/Ω , we can write

$$\left\{ \left[\frac{d(\Omega_{i1}/\Omega)/dT}{(\Omega_{i1}/\Omega)} \right]_{300 \text{ K}} \right. \\ \left. \cong (B_{\text{Ca}}^{-1} dB_{\text{Ca}}/dT)_{300 \text{ K}} - (B_{\text{Al}}^{-1} dB_{\text{Al}}/dT)_{300 \text{ K}} \right.$$

where we have neglected the relatively small term $(\beta_{\text{Ca}} - \beta_{\text{Al}})/\ln \Omega_{\text{Ca}}/\Omega$. The left-hand side of the above equation is estimated to be $-(13 \pm 4) \times 10^{-5} \text{ K}^{-1}$. As $(B_{\text{Al}}^{-1} dB_{\text{Al}}/dT)_{300 \text{ K}} = -3.6 \times 10^{-4} \text{ K}^{-1}$, we deduce $(B_{\text{Ca}}^{-1} dB_{\text{Ca}}/dT)_{300 \text{ K}} \sim -(5 \pm 0.5) \times 10^{-4} \text{ K}^{-1}$. Both the sign and order of magnitude of this quantity are entirely reasonable and fall within the range of values measured for a wide variety of metals.⁴⁵

b. Manifestation of a "Matthiessen"-type rule in thermal expansion. The fact that the calculated graph of $\Omega_i(\text{Mg})/\Omega$ vs T as well as the graph of $\Delta l - \Delta l_d$ vs T are both well described by straight lines implies that in the temperature range of interest, $\Delta\beta(\text{Mg})/C_i$ is independent of the temperature. This is strangely reminiscent of Matthiessen's rule⁴⁶ governing the change in electrical resistivity of a host metal due to the addition of an impurity. According to this rule, the resistivities contributed by two mechanisms add; that is, the extra resistance contributed by defects is very often observed to be independent of temperature. In other words, the electron-phonon interaction which gives rise to the lattice resistivity is effectively decoupled from the electron-impurity interaction defining the impurity-contributed

"extra" resistivity.

With regard to the dilatational properties of a crystal, the anharmonic part of the interionic potential gives rise to the crystal's thermal expansion as well as providing the source of the phonon-phonon interaction. The change in thermal expansion caused by an impurity may then be viewed as a change in crystal anharmonicity synonymous with the introduction of a phonon-impurity interaction that is independent of the phonon-phonon interaction described by the pure-crystal anharmonicity. Not only does the decoupling of these sources of anharmonicity take place in the dilute alloys present studied, but is equally apparent in the recent, low-temperature data for dilute CuAl alloys⁴⁷ as well. Obviously, more refined measurements on other dilute, nonmagnetic alloys have to be made to establish the generality of this result.

3. Impurity-intrinsic coefficient of thermal expansion, β_i

The calculated value of $\langle \beta_i(\text{Mg}) \rangle = 2.4 \times 10^{-4} \text{ K}^{-1}$ is in excellent agreement with the experimentally measured values of $(2.7 \pm 1.2) \times 10^{-4} \text{ K}^{-1}$ and $(1.48 \pm 0.04) \times 10^{-4} \text{ K}^{-1}$ at magnesium concentrations of 0.115 and 1.065 at. %, respectively. Thus, in both the experiment and calculation, $\langle \beta_i(\text{Mg}) \rangle / \langle \beta \rangle \sim 5$.

In contrast to magnesium, $\langle \beta_i(\text{Ca}) \rangle / \langle \beta \rangle$, as currently measured, is negative and equal to $-(3.9 \pm 1.5)$ in the temperature range explored. Again, because we lack the appropriate data for calcium, we can nevertheless make the observation that the fact that the atomic contribution to the defect volume decreases with temperature, as can be seen from Fig. 9, is not inconsistent with $\beta_i(\text{Ca}) < 0$.

VI. SUMMARY

The present interferometric, differential-length and x-ray lattice-parameter measurements in dilute AlMg and AlCa alloys yield a temperature variation of the size effect that corresponds to a relatively important disparity between the coefficient of thermal expansion of the solute atom and that of the bare solvent. Specifically, we find that even for $0.2 < T/\Theta_D < 0.4$, $\beta_i(\text{Mg})/\beta \approx 3$ and $\beta_i(\text{Ca})/\beta \approx -4$. The fact that $\beta_i(\text{Mg})$ and $\beta_i(\text{Ca})$, as well as $\Delta\beta(\text{Mg})/C_i$ and $\Delta\beta(\text{Ca})/C_i$, have opposite signs indicates that solute-solvent valence effects play a minor role in determining the solute-induced change in the solvent's thermal expansion. The complementary x-ray lattice-parameter measurements show that the size effects in the two alloys are considerably different as well, and that in the case of Mg, solute-solute interactions

are significant in determining the values of β_i , $\Delta\beta/C_i$ and Ω_i/Ω , even at C_i (Mg) ~ 0.2 at. %. Solute-solute interactions in AlCa were imperceptible for C_i (Ca)_{max} ~ 0.1 at. %.

A model calculation of the size effect and its temperature variation in the infinitely dilute alloy is presented. The volume-dependent forces are handled by means of a term describing the elastic energy associated with the solute-solvent volume misfit,^{32,33} whereas the temperature-dependent potential of Dagens *et al.*²⁹ is used to calculate the pairwise interaction between the solvent ions and the solute ion. Good agreement with the experimental data is obtained for the size effect in both AlMg and AlCa. The calculated values of $\Delta\beta$ (Mg)/ C_i and β_i (Mg) fall between the corresponding values measured in the two AlMg alloys studied. The calculation of $\Delta\beta$ (Ca)/ C_i and β_i (Ca) is not possible, due to a lack of elastic-constants data for pure, metallic calcium. The fact that the solute-solute interaction can be important at ~ 0.2 -at. % solute concentration points out that extreme care must be exercised when comparing experimental data for "dilute" alloys with calculations of infinitely dilute alloy properties.

Finally, it would appear that impurity ions, like Frenkel and Schottky defects, produce large changes in crystal anharmonicity.

ACKNOWLEDGMENTS

The authors are extremely grateful to Dr. Y. Quére of the Centres d'Etudes Nucléaires (C.E.A.) for many stimulating discussions as well as his continued encouragement concerning this work. Many hours of helpful discussions with Dr. Roger Taylor of the National Research Council of Canada regarding the theory and calculation of interionic potentials are deeply appreciated. In addition, it would indeed be a tremendous oversight to not mention the extremely valuable advice relating to various aspects of interferometric length measurement given to us by Dr. B. Yates of the University of Salford, England. We are indebted to both the C.E.A., France, and the Centre National de Recherche Scientifique (C.N.R.S.), France, for their joint support of this project.

APPENDIX A: CALCULATION OF FIRST- AND SECOND-NEAREST-NEIGHBOR RELAXATION DISPLACEMENTS

The force-constant matrix $\phi(l)$ of the perfect crystal is obtained from the first and second derivatives of the pairwise Al ion-Al ion interaction potential Φ evaluated at the equilibrium positions:

$$\phi_{\alpha\beta}(l) = r_{\alpha i} r_{\beta i} r_i^{-2} [r_i^{-1} \Phi'(r_i) - \Phi''(r_i)] - \delta_{\alpha\beta} r_i^{-1} \Phi'(r_i).$$

The static Green's function $G(l)$ of the perfect crystal is then obtained by taking the inverse Fourier transformation of $\phi^{-1}(k)$ where $\phi(k)$ is the Fourier transformation of $\phi(l)$ and is calculated for each of the allowed values (25 000) of the wave vector in the symmetry-reduced part ($\frac{1}{8}$) of the Brillouin zone for l spanning the first eight nearest-neighbor shells. We assume that the act of replacing an aluminum atom by an impurity is felt only by the first- and second-nearest neighbors of the impurity. The force-constant matrix $\phi^*(l)$ of the imperfect crystal can then be written as

$$\phi^*(l) = \phi(l) - \delta\phi(l),$$

where

$$\delta\phi(l) = \begin{cases} \phi_{Al-Al} - \phi_{Al-S}, & l=1, 2 \\ 0, & l \geq 3 \end{cases}$$

The Green's function of the dilute alloy is then given by

$$\underline{G}^* = (\underline{I} - \underline{G} \delta\phi)^{-1} \underline{G},$$

where G is the perfect-crystal Green's function. The atomic, relaxation displacements u in the perturbed region are evaluated by means of

$$\underline{u} = \underline{G}^* \underline{F},$$

where

$$\underline{F} = -\underline{\nabla} \Psi|_{r_i}, \quad l=1, 2.$$

At $T=140$ K, the center of the explored temperature range, the first- and second-nearest-neighbor displacements for Mg and Ca are found to be $u_1/a = -1.6 \times 10^{-4}$, $u_2/a = -5.3 \times 10^{-4}$, and $u_1/a = 7.8 \times 10^{-3}$, $u_2/a = -4.2 \times 10^{-3}$, respectively.

APPENDIX B: CONTRIBUTION OF THE DIFFERENTIAL-LENGTH AND LATTICE-PARAMETER UNCERTAINTIES TO $\delta\beta_i$

From Eq. (18), for $\langle\beta_i - \beta\rangle (T_U - T_L) \ll 1$, we obtain the following expression for $\delta\beta_i/\beta_i$:

$$\frac{\delta\beta_i}{\beta_i} \cong \frac{4}{5} \left(\frac{\delta(\Delta l - \Delta l_d)}{(\Delta l - \Delta l_d)} + \frac{\delta\Delta a}{\Delta a} + \frac{\delta\langle\beta\rangle}{4\langle\beta\rangle} \right), \quad (B1)$$

where we have taken as representative $(1/C_i)(\Delta a/a_0)c_i \sim 10^{-1}$, $C_i \sim 10^{-2}$, $a_0 \sim 4$ Å, and $\delta a \sim 10^{-4}$ Å. We have obviously dropped the relatively negligible terms $\delta l/l$, $\delta\Delta T/\Delta T$, and $\delta a_0/a_0$. In addition, we have taken $\langle\beta_i\rangle \sim 5\langle\beta\rangle$. As $\delta\beta/\beta \sim 5 \times 10^{-2}$ for $\delta(\Delta l - \Delta l_d) \sim 3 \times 10^{-2}$ μm, and $\Delta l - \Delta l_d \sim 0.5$ μm, Eq. (B1) yields $\delta\beta_i/\beta_i \sim 10\%$.

APPENDIX C: MAXIMUM ALLOWED DIFFERENCE ϵ
BETWEEN THE SAMPLE AND DUMMY LENGTHS

We can obviously write

$$l_d = l + \epsilon. \quad (C1)$$

From Eq. (C1) and to first order in ϵ ,

$$l_d^{-1} = l^{-1} - \epsilon l^{-2}. \quad (C2)$$

Using Eq. (C2) together with the definition of the difference between the sample and dummy fractional-length changes, we obtain

$$\begin{aligned} \Delta l/l - \Delta l_d/l_d &= \Delta l/l - (\Delta l_d/l - \epsilon \Delta l_d/l^2) \\ &= (\Delta l - \Delta l_d)/l + \epsilon \Delta l_d/l^2. \end{aligned} \quad (C3)$$

Evidently, in the present context, $\delta(\Delta l/l - \Delta l_d/l_d) = \epsilon \Delta l_d/l^2$. Using this relation in Eq. (B1) yields

$$\delta \beta_i / \beta_i \cong 0.8 (\epsilon \Delta l_d / l^2) / [(\Delta l - \Delta l_d) / l]. \quad (C4)$$

Taking $\langle \beta \rangle = 3 \times 10^{-5} \text{ K}^{-1}$ in the temperature range defined by $T_L = 80 \text{ K}$ and $T_U = 180 \text{ K}$, $\Delta l/l = \langle \beta \rangle (T_U - T_L) = 3 \times 10^{-5} \times 100 = 3 \times 10^{-3}$. To a very good approximation, the quantity $\Delta l_d/l^2$ can be replaced by $\Delta l/l^2$ in Eq. (C4). Taking $\Delta l - \Delta l_d = 0.5 \text{ } \mu\text{m}$ and $\epsilon = 5 \text{ } \mu\text{m}$, Eq. (C4) yields $\delta \beta_i / \beta_i \cong 3\%$. Thus, the left-hand side of Eq. (18) can be replaced by the left-hand side of Eq. (19) with little error.

APPENDIX D: UNCERTAINTY ASSOCIATED
WITH THE THERMAL EXPANSION OF THE QUARTZ
OPTICAL DISKS

In the temperature range where the experiments are performed, the linear coefficient of thermal expansion of quartz is $\alpha_q = 2 \times 10^{-7} \text{ K}^{-1}$. This means that when the temperature changes by 100 K, the separation S_q between S_1 and S_2 , typically about 50 μm , changes by $\Delta S_q = S_q \alpha_q (T_U - T_L) = 50 \times 2 \times 10^{-7} \times 100 = 10^{-3} \text{ } \mu\text{m}$. As $\Delta l - \Delta l_d \cong 0.5 \text{ } \mu\text{m}$ the

dilatation of the optical disks thus contributes a relatively negligible uncertainty to β_i of the order of $10^{-3}/0.5 = 0.2\%$.

APPENDIX E: MAXIMUM ALLOWED VARIATION
IN SAMPLE-DUMMY TEMPERATURE
DIFFERENCE, ΔT_{SD}

It is obvious that even when the sample and dummy are identical in every respect, a variation ΔT_{SD} in their temperature difference in the temperature range $T_L \leq T \leq T_U$ will cause an apparent differential length change, $\delta(\Delta l - \Delta l_d)$, given by

$$\delta(\Delta l - \Delta l_d) = \langle \beta \rangle l \Delta T_{SD} / 3. \quad (D1)$$

Due to this source of error, between Eqs. (B1) and (D1) we obtain, for $\delta \beta_i / \beta_i$,

$$\begin{aligned} \delta \beta_i / \beta_i &= 0.8 \delta(\Delta l - \Delta l_d) / (\Delta l - \Delta l_d) \\ &= \langle \beta \rangle l \Delta T_{SD} / 3 (\Delta l - \Delta l_d). \end{aligned} \quad (D2)$$

For $\langle \beta \rangle = 3 \times 10^{-5} \text{ K}^{-1}$, $l = 5 \times 10^4 \text{ } \mu\text{m}$, $\Delta l - \Delta l_d = 0.5 \text{ } \mu\text{m}$, and $\delta \beta_i / \beta_i = 3\%$, $\Delta T_{SD} \cong 40 \text{ mK}$. In all of the runs performed, ΔT_{SD} never exceeded 25 mK.

APPENDIX F: UNCERTAINTY IN THE X-RAY
SIZE-EFFECT MEASUREMENTS

The lattice parameters are presently measured to $\pm 10^{-4} \text{ } \text{Å}$, whereas the solute concentrations are known to within $\sim 1\%$. The fractional uncertainty in the size effect is thus given by $\delta \Delta a / \Delta a$. As can be seen from Table III, for $C_i (\text{Mg}) = 0.115 \text{ at. } \%$, $\Delta a = 4.0490 - 4.0488 \text{ } \text{Å} = 2 \times 10^{-4} \text{ } \text{Å}$, so that $\delta \Delta a / \Delta a = 1 \times 10^{-4} \sqrt{2} / 2 \times 10^{-4} = 70\%$. On the other hand, the most precise measurement of the size effect occurs for $C_i (\text{Mg}) = 1.065 \text{ at. } \%$. In this case $\Delta a = 4.0535 - 4.0488 \text{ } \text{Å} = 47 \times 10^{-4} \text{ } \text{Å}$, and $\delta \Delta a / \Delta a = 1 \times 10^{-4} \sqrt{2} / 47 \times 10^{-4} = 3\%$. The uncertainties in the size-effect measurements on the AlCa alloys studied fall between these extremes.

*Present address: Laboratoire Léon Brillouin, B. P. 2, 91190 Gif-sur-Yvette, France.

[†]Present address: DTech/STA-Centre d'Etudes Nucléaires de Saclay, B. P. 2, 91190 Gif-sur-Yvette.

¹P. C. Gehlen, J. R. Beeler and R. I. Jaffee, *Interatomic Potentials and Simulations of Lattice Defects* (Plenum, New York, 1972).

²H. M. Gilder and L. C. Chhabildas, *Phys. Rev. Lett.* **26**, 1027 (1971).

³C. H. Leung and M. J. Stott, *J. Phys. F* **7**, 1651 (1977).

⁴P. Audit and H. M. Gilder, *Phys. Rev. B* **18**, 4151 (1978).

⁵L. M. Levinson and F. R. N. Nabarro, *Acta Metall.* **15**, 785 (1967).

⁶L. A. Girifalco, *Scripta Metall.* **1**, 5 (1967).

⁷H. M. Gilder and D. Lazarus, *Phys. Rev. B* **11**, 4916 (1975).

⁸J. N. Mundy, *Phys. Rev. B* **3**, 2431 (1971).

⁹L. C. Chhabildas and H. M. Gilder, *Phys. Rev. B* **5**, 2135 (1972).

¹⁰B. J. Buescher, H. M. Gilder, and N. Shea, *Phys. Rev. B* **7**, 2261 (1973).

¹¹J. P. Ganne and J. von Stebut, *Phys. Rev. Lett.* **43**, 634 (1979).

¹²W. B. Pearson, *Handbook of Lattice Spacings and Structure of Metals and Alloys* (Pergamon, London, 1967).

¹³P. S. Turner, *J. Res. Nat. Bur. Stand.* **37**, 239 (1946).

- ¹⁴J. D. Eshelby, *J. Appl. Phys.* **25**, 255 (1954).
- ¹⁵T. J. Hughes and J. C. Brittain, *Phys. Rev. A* **135**, 1738 (1964).
- ¹⁶A. B. Blandin and S. L. Déplante, *J. Phys. Radium* **23**, 609 (1962).
- ¹⁷J. L. Déplante and A. Blandin, *J. Phys. Chem. Solids* **26**, 381 (1965).
- ¹⁸L. I. Ivanov, Y. M. Platov, and M. N. Pletnev, *Phys. Status Solidi B* **64**, 771 (1974).
- ¹⁹R. Visnov and L. A. Girifalco, *J. Phys. Chem. Solids* **40**, 449 (1979).
- ²⁰See, for example, *Thermal Expansion—1971 (Corning)*, Proceedings of the Thermal Expansion Symposium, edited by M. G. Graham and H. E. Hagy (AIP, New York, 1972).
- ²¹J. A. Khan and D. Griffiths, *J. Phys. F* **8**, 763 (1978).
- ²²H. J. Axon and W. Hume-Rothery, *Proc. R. Soc. London A* **193**, 1 (1948).
- ²³A. Z. Zhmudskiy, P. A. Maksimiyuk, V. D. Mikhalko, and V. A. Gley, *Fiz. Met. Metalloved.* **27**, 373 (1969).
- ²⁴A. C. Bailey, N. Waterhouse, and B. Yates, *J. Phys. C* **2**, 769 (1969).
- ²⁵W. Hume-Rothery and Boulton, *Philos. Mag.* **40**, 71 (1949).
- ²⁶D. R. Beaman, R. W. Balluffi, and R. O. Simmons, *Phys. Rev.* **137**, A917 (1965).
- ²⁷H. M. Gilder, *Bull. Am. Phys. Soc.* **24**, 272 (1979).
- ²⁸A. C. Bailey, N. Waterhouse, and B. Yates, *J. Phys. C* **2**, 769 (1969).
- ²⁹L. Dagens, M. Rasolt, and R. Taylor, *Phys. Rev. B* **11**, 2726 (1975).
- ³⁰P. Beauchamp, R. Taylor, and V. Vitek, *J. Phys. F* **5**, 2017 (1975).
- ³¹A. Blandin and J. L. Déplante, *Metallic Solid Solutions* (Benjamin, New York, 1963), p. IV-1.
- ³²T. M. Hayes and W. H. Young, *Philos. Mag.* **21**, 583 (1970).
- ³³J. A. Alonso and L. A. Girifalco, *J. Phys. F* **8**, 2455 (1978).
- ³⁴H. M. Gilder and P. Audit, *Phys. Rev. Lett.* **38**, 30 (1977).
- ³⁵V. K. Tewary, *Adv. Phys.* **22**, 757 (1973).
- ³⁶M. Rasolt and R. Taylor, *J. Phys. F* **7**, 47 (1977).
- ³⁷G. Simmons and H. Wang, *Single Crystal Elastic Constants and Calculated Aggregate Properties* (MIT, Cambridge, Mass., 1971).
- ³⁸M. S. Duesbery and R. Taylor, *J. Phys. F* **7**, 47 (1977).
- ³⁹V. K. Afanas'yev, *Krasnoyarsk. kn. izd-vo*, **6**, 121 (1972).
- ⁴⁰F. A. Jenkins and H. E. White, *Fundamentals of Optics* (McGraw-Hill, New York, 1957), p. 266.
- ⁴¹E. R. Peck and S. W. Obetz, *J. Opt. Soc. Am.* **43**, 505 (1953).
- ⁴²W. R. C. Rowly, *IEEE Trans. Instrum. Meas.* **IM-15**, 4, 146 (1966).
- ⁴³*American Institute of Physics Handbook*, edited by D. E. Gray (McGraw-Hill, New York, 1972).
- ⁴⁴D. M. Poole and H. J. Axon, *J. Inst. Met.* **80**, 599 (1952).
- ⁴⁵H. B. Huntington, *Solid State Phys.* **7**, 213 (1958).
- ⁴⁶A. Matthiessen, *Rep. Br. Assoc. Adv. Sci.* **32**, 144 (1862).
- ⁴⁷J. P. Ganne, *J. Phys. (Paris) Lett.* **40**, L-481 (1979).